REGULAR ARTICLE

blood advances

Distinct peripheral T-cell and NK-cell profiles in HGBL-*MYC/BCL2* vs patients with DLBCL NOS

A. Vera de Jonge,[1,2] Carolien Duetz,[1,2] Wassilis S. C. Bruins,[1,2] Charlotte L. B. M. Korst,[1,2] Rosa Rentenaar,[1,2] Meliha Cosovic,[1,2] Merve Eken,[1,2] Inoka Twickler,[1,2] Marcel Nijland,[4] Marjolein W. M. van der Poel,[5] Koen de Heer,[3] Clara P. W. Klerk,[6] Leonie Strobbe,[7] Margriet Oosterveld,[8] Rinske Boersma,[9] Harry R. Koene,[10] Margaretha G. M. Roemer,[1,2] Erik van Werkhoven,[11,12] Martine E. D. Chamuleau,[1,2] and Tuna Mutis[1,2]

[1]Department of Hematology, Amsterdam UMC Location Vrije Universiteit, Amsterdam, The Netherlands; [2]Cancer Center Amsterdam, Cancer Biology and Immunology, Amsterdam, The Netherlands; [3]Department of Internal Medicine, Flevoziekenhuis, Almere, The Netherlands; [4]Department of Hematology, University Medical Center Groningen, Groningen, The Netherlands; [5]Division of Hematology, Department of Internal Medicine, GROW School for Oncology and Developmental Biology, Maastricht University Medical Center, Maastricht, The Netherlands; [6]Department of Internal Medicine, Dijklanderziekenhuis, Hoorn, The Netherlands; [7]Department of Internal Medicine, Gelreziekenhuizen, Zutphen, The Netherlands; [8]Department of Internal Medicine, CWZ, Nijmegen, The Netherlands; [9]Department of Internal Medicine, Amphia Ziekenhuis, Breda, The Netherlands; [10]Department of Hematology, St Antonius Ziekenhuis, Nieuwegein, The Netherlands; [11]HOVON Foundation, Rotterdam, The Netherlands; and [12]Department of Hematology, Erasmus MC Cancer Institute, Rotterdam, The Netherlands

Key Points

- Distinct peripheral T-cell and NK-cell phenotypes exist in patients with HGBL-*MYC/BCL2* vs patients with DLBCL NOS without *MYC* rearrangements.
- Patients with HGBL-*MYC/BCL2* encompass exhausted PD-1$^+$ T cells without other immune effector cell impairments.

Patients with high-grade B-cell lymphoma with *MYC* and *BCL2* rearrangements (HGBL-*MYC/BCL2*) respond poorly to immunochemotherapy compared with patients with diffuse large B-cell lymphoma not otherwise specified (DLBCL NOS) without a *MYC* rearrangement. This suggests a negative impact of lymphoma-intrinsic *MYC* on the immune system. To investigate this, we compared circulating T cells and natural killer (NK) cells of patients with HGBL-*MYC/BCL2* (n = 66), patients with DLBCL NOS (n = 53), and age-matched healthy donors (HDs; n = 16) by flow cytometry and performed proliferation, cytokine production, and cytotoxicity assays. Compared with HDs, both lymphoma subtypes displayed similar frequencies of CD8$^+$ T cells but decreased CD4$^+$ T cells. Regulatory T-cell (Treg) frequencies were reduced only in patients with DLBCL NOS. Activated (HLA-DR$^+$/CD38$^+$) T cells, PD-1$^+$CD4$^+$ T cells, and PD-1$^+$Tregs were increased in both lymphoma subtypes, but PD-1$^+$CD8$^+$ T cells were increased only in HGBL-*MYC/BCL2*. Patients with DLBCL NOS, but not patients with HGBL-*MYC/BCL2*, exhibited higher frequencies of senescent T cells than HDs. Functional assays showed no overt differences between both lymphoma groups and HDs. Deeper analyses revealed that PD-1$^+$ T cells of patients with HGBL-*MYC/BCL2* were exhausted with impaired cytokine production and degranulation. Patients with DLBCL NOS, but not patients with HGBL-*MYC/BCL2*, exhibited higher frequencies of NK cells expressing inhibiting receptor NKG2A. Both lymphoma subtypes exhibited lower TIM-3$^+$– and DNAM-1$^+$–expressing NK cells. Although NK cells of patients with HGBL-*MYC/BCL2* showed less degranulation, they were not defective in cytotoxicity. In conclusion, our results demonstrate an increased exhaustion in circulating T cells of patients with HGBL-*MYC/BCL2*. Nonetheless, the overall intact peripheral T-cell and NK-cell functions in these patients emphasize the importance of investigating potential immune evasion in the microenvironment of *MYC*-rearranged lymphomas.

Submitted 14 September 2023; accepted 22 December 2023; prepublished online on *Blood Advances* First Edition 8 January 2024; final version published online 28 February 2024. https://doi.org/10.1182/bloodadvances.2023011687.

Data are available in the main text or the supplemental materials.

Original data are available upon reasonable request from the corresponding author, Tuna Mutis (t.mutis@amsterdamumc.nl).

The full-text version of this article contains a data supplement.

Introduction

MYC translocations are prevalent genetic aberrations in patients with aggressive B-cell lymphoma (BCL). The 2022 HAEM5 World Health Organization (WHO) classification defines patients with both *MYC* and *BCL2* rearrangements (without additional *BCL6* translocation [double hit (DH)] or with [triple hit (TH)]) as diffuse large BCL (DLBCL)/high-grade BCL (HGBL) with *MYC* and *BCL2* rearrangements (HGBL-*MYC/BCL2*).[1] Patients without a *MYC* rearrangement are referred to as diffuse and high-grade large BCL not otherwise specified (DLBCL NOS). Patients with HGBL-*MYC/BCL2* patients often exhibit an aggressive clinical course with lower response rates and increased resistance toward standard first-line immunochemotherapy with rituximab, cyclophosphamide, doxorubicin, vincristine, and prednisone (R-CHOP).[2-4] Emerging immunotherapeutic approaches, such as bispecific or trispecific T-cell engagers or chimeric antigen receptor T-cell therapy, have shown promise for patients with R-CHOP resistance.[5-11] Response to immunotherapy is influenced by various factors, including tumor-intrinsic molecular and genetic characteristics, the tumor microenvironment, and the host systemic immune response.[12,13] Theoretically, *MYC* can affect each of these factors.

Different studies have suggested a role for MYC in modulating peripheral immune cells in lymphoma. A murine model of T-cell lymphoma suggests that MYC modulates the tumor microenvironment by suppressing natural killer (NK) cell numbers and the expression of activating NK cell marker NKp46.[14] Studies on small sets of patients with *MYC*-rearranged lymphoma reported decreased $CD3^+$ T cells compared with healthy donors (HDs)[15] and higher frequencies of $CD4^+CD8^+$ T cells and γδ T cells than patients with DLBCL NOS but a lower ratio of immunosuppressive $CD4^-CD8^-$ T-cells.[16] However, studies extensively investigating the impact of oncogenic *MYC* on phenotype and functionality of circulating immune effector cells in patients with HGBL-*MYC/BCL2* vs those with DLBCL NOS are lacking. In light of current and emerging T-cell– and NK cell–based immunotherapeutic approaches, we performed comprehensive flow cytometry–based profiling of circulating peripheral blood T cells and NK cells from a large cohort of newly diagnosed patients with HGBL-*MYC/BCL2* and compared them with newly diagnosed patients with DLBCL NOS without a *MYC* rearrangement and age-matched HDs.

Methods

Patients, sample collection, and sample verification

Peripheral blood samples from patients with HGBL-*MYC/BCL2* were collected in heparinized tubes between August 2018 and December 2022 from patients included in the HOVON-152 trial (NCT03620578). In this trial, 1 cycle of R-CHOP or dose-adjusted (etoposide, prednisone, vincristine, cyclophosphamide, doxorubicin, and rituximab [DA-EPOCH-R]) before enrollment was allowed. Peripheral blood samples were collected after the first cycle of R-CHOP or DA-EPOCH-R (day 1 of the second cycle). In the HOVON-152 trial, patients with DH or TH HGBL were included based on the revised fourth edition of the WHO classification (2016).[17] Yet, for this analysis, we excluded BCL6 DH cases, focusing solely on HGBL-*MYC/BLC2* cases as per the updated 2022 HAEM5 WHO classification.[1]

Peripheral blood samples from patients with DLBCL NOS were collected in heparinized tubes between April 2020 and December 2020 from patients included in the HOVON-902 (NCT04139252) observational cohort. In this cohort, samples were collected on day 1 of the first cycle and day 1 of the second cycle of R-CHOP (21 days).

The study protocols were approved by the local medical ethics committee of the Amsterdam UMC (HOVON-152: *NL63247.029.17*; HOVON-902: CCMO *NL70323.029.19)* and conducted in accordance with the Declaration of Helsinki. All patients provided written informed consent before participating in the studies. Additional information about the HOVON-152 trial and HOVON-902 cohort is provided in the supplemental Materials.

Peripheral blood samples from HDs were obtained from Sanquin (Amsterdam, The Netherlands). Sanquin is the central Dutch organization authorized to supply blood products. Donations are on a voluntary, nonremunerated basis and include written informed consent as part of routine donor selection. We selected peripheral blood samples from 16 HDs with a similar median age (64 years) as the patients with HGBL-*MYC/BCL2* and DLBCL NOS.

Cell culture

K562 (CCL-243) cell line was purchased from the American Tissue Culture Collection and cultured in RPMI-1640 (Gibco, Thermo Fisher, 524000025), supplemented with 10% heat-inactivated fetal bovine serum (Invitrogen) and 1% penicillin/streptomycin (Invitrogen, 15140122). Authenticity was verified by short-tandem repeat profiling (GenePrint 10 System Promega). K562 was cultured for not more than 2 months and tested negative for mycoplasma contamination before use.

Processing of human peripheral blood samples

Peripheral blood samples were processed centrally at the Amsterdam University Medical Center within 48 hours of collection. Peripheral blood mononuclear cells (PBMCs) were isolated from whole blood using density gradient centrifugation with Ficoll-Paque Plus (Sigma-Aldrich; GE17-1440-03). PBMCs aliquots were stored in liquid nitrogen until further analysis.

Flow cytometry–based immunophenotyping of PBMCs

Cryopreserved PBMCs of patients, HDs, and a reference control that was included for each staining (buffy coat obtained from Sanquin, The Netherlands) were thawed at 37°C, washed once with Iscove's Modified Dulbecco's Medium-medium supplemented with 20% fetal calf serum (FCS) and antibiotics (100 U/mL penicillin; 100 μg/mL streptomycin), treated with DNase (Roche, catalog no. 10104159001) for 5 minutes, washed, and resuspended in warm Iscove's Modified Dulbecco's Medium before automatically evaluating cell viability using acridine orange/propidium iodide. Cells were cultured for 16 hours at 2×10^6 to 5×10^6 viable cells per mL in 37°C and 5% CO_2 for cell recovery and to allow upregulation of cell surface markers affected by cryopreservation. After re-evaluating cell viability with acridine orange/propidium iodide, the cells were stained with a cell viability dye. Median cell viability was 71.5% and 82.2% for patients and HDs, respectively. Multicolor panels (0.5×10^6-1×10^6 viable cells per panel) with predefined, validated fluorochrome-conjugated antibody combinations are listed in supplemental Table 1. Human normal immunoglobulins (final concentration 0.1 mg/mL; Nanogam, Sanquin Plasma

Products B.V.) were added before staining to reduce unwanted nonspecific FC-receptor binding of fluorochrome-conjugated antibodies. Cells were then washed in phosphate buffer saline (PBS) + 0.1% human serum albumin and analyzed using a 5-laser LSRFortessa flow cytometer (Becton Dickinson).

Spectral overlap was automatically calculated and compensated using compensation beads and FACSDiva software. Flow cytometer performance and standardization were monitored daily with fluorescent-labeled CS&T beads (BD, 655051). Laser voltages were optimized within a <2% deviation using BD OneFlow Setup Beads (BD, 658620) and Alignflow Flow cytometry Alignment Beads (Thermo Fisher Scientific, A16502) on a daily setting.

Manual pregating and computational analysis

Raw flow cytometric data of immunophenotyping (fcs 3.1 files) were manually analyzed using FCS Express Flow Cytometry Software version 6 to identify, gate, and export single T-cell and NK-cell populations. These cells were preprocessed (included data cleaning using PeacoQC,[18] hyperbolic arcsin transformation, approximated min-max scaling, and batch correction using quantile normalization) and analyzed in R and Rstudio version 4.0.3. Computational data analysis was performed using Uniform Manifold Approximation and Projection (UMAP) and FlowSOM on 10 000 cells per fcs file. For the FlowSOM analysis, the number of metaclusters was optimized until all metaclusters were either negative or positive for a particular marker. Then, the complete fcs files were mapped on the optimized FlowSOM to calculate metacluster percentages per sample. Based on marker expression of all metaclusters, percentages of T-cell and NK-cell subsets (supplemental Table 2) and individual marker expression were calculated.

T-cell proliferation

Cryopreserved PBMCs were thawed as described above. Cell concentration and viability were counted using trypan blue staining (82% and 94% cell viability for patients and HDs, respectively). PBMCs were immediately stained with Cell Tracer Violet (CTV, Invitrogen, C34557) according to manufacturer's protocol, seeded in 96-wells U bottom plates (0.1×10^6 live cells per well in triplicate) and stimulated with CD3xCD28 Dynabeads (DynabeadsTM Human T-activator CD3/CD28; Thermo Fisher Scientific, 11131D) at a bead-to-cell ratio of 1:5 for 5 days at 37°C and 5% CO_2. Unstimulated cells and non-CTV–labeled cells were simultaneously incubated as experimental controls.

After incubation, cells were collected, and beads were magnetically removed. Triplicates were pooled and cells were stained with antibodies (supplemental Table 3) and measured on a 5-laser LSRFortessa (Becton Dickinson) flow cytometer. Flow-Count Fluorospheres (Beckman Coulter, 7547053) were added to allow equalized measurements of T cells between tubes/samples. Proliferation of T-cell subsets were analyzed using the proliferation analysis tool in FCS Express version 6. The division index (fold expansion over time for responding cells) and the proliferation index (average number of divisions that responding cells have undergone) were defined as described elsewhere.[19]

T-cell intracellular cytokine production and degranulation

PBMCs were seeded in 96-wells U bottom plates (0.5×10^6 live cells per well in duplicate) and stimulated with phorbol 12-myristate-13-acetate (PMA)/ionomycin (1:500) for 4 hours at 37°C and 5% CO_2 in the presence of an anti-human CD107a (PE) antibody. During the last 3 hours of incubation, brefeldin A/monensin (1:1000) were added. Thereafter, duplicate wells were pooled, transferred to 5 mL FACS tubes, and washed once in PBS. Extracellular staining was done with a panel of antibodies specific for human cell surface markers (supplemental Table 4). After washing in PBS + 0.1% human serum albumin, cells were fixed and permeabilized using fixation buffer (Biolegend, catalog no. 420801) and intracellular staining permeabilization wash buffer (Biolegend, catalog no. 421002) according to manufacturer's instructions.

Cells were intracellularly stained with antibodies targeted against interferon gamma (IFN-γ), tumor necrosis factor alpha (TNF-α), and interleukin-2 (IL-2) (supplemental Table 4). After washing once in permeabilization buffer, cells were measured on a 5-laser LSRFortessa (Becton Dickinson) flow cytometer. The percentage of total $CD4^+$ and $CD8^+$ as well as PD-1^+CD4^+ and PD-1^+CD8^+ T cells positive for IFN-γ, TNF-α, and IL-2 was calculated in comparison with the unstimulated cells.

NK-cell cytotoxicity and degranulation

Cryopreserved PBMCs were thawed as described above and cells were rested overnight at 2×10^6 to 5×10^6 viable cells per mL in 37°C and 5% CO_2 to allow for functional recovery of NK cells. The next day, K562 cells were stained with CTV according to manufacturer's protocol and seeded as target cells in 96-wells U bottom plates (0.02×10^6 live cells per well, in triplicates). PBMC (0.4×10^6 live cells per well) were added to K562 cells in duplicates, whereas single K562 wells served as negative control to calculate lysis. Anti-CD107 antibodies (anti-CD107a and anti-CD107b, both FITC; BD catalog no. 555800 and 555804, respectively) were added. $K562^+$ PBMC wells without anti-CD107a/b antibodies were simultaneously incubated as full minus one controls. Cells were incubated for 4 hours at 37°C and 5% CO_2. After incubation, surviving K562 target cells were enumerated by standard quantitative flow cytometry on a 4-laser FACS Celesta (Becton Dickinson) flow cytometer. K562 viability was determined using LIVE/DEAD Fixable NEAR-IR Dead Cell Stain (Invitrogen, L10119), and PBMCs were identified through additional labeling with a defined antibody set (supplemental Table 5). Flow volume control was done by adding Flow-Count Fluorospheres (Beckman Coulter, 7547053).

The percent lysis of K562 (target) cells was calculated according to the following formula: % lysis = 1 − (absolute number of surviving cells in treated wells)/(absolute number of surviving cells in K562 only wells) × 100%. Degranulation was measured as percentage of NK cells positive for CD107a/b surface expression based on full-minus-one control.

Statistical analysis

Data were analyzed and visualized using FCS Express Flow Cytometry Software (De Novo Software versions 06.0025 and 7.14.0020), GraphPad Prism 8.2.1, and RStudio version 4.0.3.

Paired data of samples before and after R-CHOP or unstimulated and stimulated samples were analyzed using a Student paired *t* test with *P* value <.05 as statistical significance threshold. No multiple correction was applied.

For nonparametric distributions, Mann-Whitney *U* tests were used to compare patients with HGBL-*MYC/BCL2* with those with DLBCL NOS (primary comparison) and for comparing the lymphoma groups with HDs, with *P* value <.05 as statistical significance threshold. The Benjamin-Hochberg procedure for multiple testing was applied to control the false discovery rate for comparisons of the FlowSOM clusters.

To correct for baseline characteristics that were significantly different between patients with HGBL-*MYC/BCL2* and patients with DLBCL NOS (age, WHO performance score, and International Prognostic Index [IPI] group), linear regression analysis was performed on immune cell subsets that significantly differed between lymphoma subtypes ($CD4^{-}CD8^{-}$ T-cells, regulatory T cells [Tregs], γδ T cells, $PD\text{-}1^{+}CD8^{+}$ T cells, T cells with a senescent phenotype, and NKG2A-expressing NK cells).

Results

We randomly selected samples from patients with HGBL-*MYC/BCL2* (n = 66) and patients with DLBCL NOS (n = 53) based on sample availability to investigate their peripheral blood T cells and NK cells. Baseline characteristics of both lymphoma subtypes are presented in Table 1. Patients with HGBL-*MYC/BCL2* were younger (median age, 60.2 years) than patients with DLBCL NOS (median age, 67.0 years; $P < .001$, Wilcoxon signed-rank test), more often had a lower WHO performance score ($P = .048$, χ^2 test), and more often a low-intermediate or high-intermediate IPI score ($P = .04$).

Table 1. Baseline characteristics

	HGBL-*MYC/BCL2* (n = 66)	DLBCL NOS (n = 53)	*P* value
Age, y			
Mean (SD)	60.2 (9.78)	67.0 (11.2)	<.001
Median (min, max)	62.0 (35.0, 79.0)	68.0 (32.0, 88.0)	
Sex			
Male	42 (63.6%)	28 (52.8%)	.32
Female	24 (36.4%)	25 (47.2%)	
WHO performance score			
0	43 (65.2%)	26 (49.1%)	.048
1	19 (28.8%)	15 (28.3%)	
2	4 (6.1%)	10 (18.9%)	
3	0 (0%)	2 (3.8%)	
LDH level			
Within normal range	21 (31.8%)	23 (43.4%)	.27
Elevated	45 (68.2%)	30 (56.6%)	
Extranodal localizations (number)			
None	25 (37.9%)	20 (37.7%)	.5
1	14 (21.2%)	14 (26.4%)	
≥2	26 (39.4%)	14 (26.4%)	
Unknown	1 (1.5%)	5 (9.4%)	
IPI score			
Low	8 (12.1%)	11 (20.8%)	.04
Low-intermediate	28 (42.2%)	15 (28.3%)	
High-intermediate	24 (36.4%)	14 (26.4%)	
High	6 (9.1%)	9 (17.0%)	
Missing	0 (0%)	4 (7.5%)	
***MYC*-rearrangement**			
No		53 (100%)	
Yes	66 (100%)		
DH/TH status			
HGBL: BCL2 DH	52 (78.8%)		
HGBL: TH	14 (21.2%)		
DLBCL NOS		53 (100%)	

LDH, lactate dehydrogenase; TH, triple hit.

Effect of 1 cycle of R-CHOP on peripheral T cells and NK cells

In this study, samples of patients with HGBL-*MYC/BCL2* and patients with DLBCL NOS were compared after 1 cycle of R-CHOP (supplemental Figure 1A). As a study prerequisite, potential confounding effects of R-CHOP on T cell and NK cell populations were assessed in patients with DLBCL NOS by comparing samples before and after 1 cycle of R-CHOP21 (blood samples collected at the first day of cycle 1 and first day of cycle 2, respectively). Although frequencies of LAG3-expressing $CD4^+$ T cells and Tregs, TIM-3–expressing $CD8^+$ T cells, and PD-1^+ γδ T cells were decreased (supplemental Figure 2A), 1 cycle of R-CHOP did not affect the frequency of major T-cells populations (supplemental Figure 2B), the distribution of T-cell differentiation states (naïve, stem cell memory, central memory, effector memory T-cells, and terminally differentiated effector memory T cells re-expressing CD45RA; supplemental Figure 2C), and the fraction of $CD4^+$ and $CD8^+$ T cells expressing markers associated with T-cell senescence (loss of CD27 and CD28, and gain of KLRG1 and CD57; supplemental Figure 2D). The frequency of $CD4^+$ expressing activation marker CD38 was increased after 1 cycle of R-CHOP, but the frequencies of $CD4^+$ and $CD8^+$ T cells expressing other activation markers (CD25 and HLA-DR) remained unaffected (supplemental Figure 2E).

NK cells could only be analyzed in a maximum of 51 of 66 patients with HGBL-*MYC/BCL2*, 35 of 53 patients with DLBCL NOS, and 15 of 16 HDs due to limited cell numbers (supplemental Figure 1B). There was no impact of 1 cycle of R-CHOP on activation NK cell markers or inhibiting or activating NK cell receptors (supplemental Figure 3A-C), except for a decrease in $CD16^+$ NK cells and increase in $CD56^{bright}$ NK cells (supplemental Figure 3D), as could be expected after the antibody-dependent cellular cytotoxicity effects of rituximab via the Fc-γ receptor IIIa (CD16) on NK cells.

Similar T-cell subset distribution in patients with HGBL-*MYC/BCL2* and HDs but decreased Treg frequency in DLBCL NOS

We analyzed the T-cell compartment of patients with HGBL-*MYC/BCL2,* patients with DLBCL NOS, and age-matched HDs. Total white blood cell count (supplemental Figure 4A) and frequencies of $CD8^+$ T cells were similar between both lymphoma groups and HDs. $CD4^+$ T-cell frequencies decreased in both lymphoma subtypes compared with HDs (Figure 1A). Interestingly, the majority of patients with DLBCL NOS showed decreased Treg frequencies and increased $CD4^-CD8^-$ T-cell frequencies compared with patients with HGBL-*MYC/BCL2* and HDs (Figure 1A). In some of the patients with DLBCL NOS, the increase in $CD4^-CD8^-$ T cells was reflected in increased γδ T-cell frequencies compared with that of patients with HGBL-*MYC/BCL2* (Figure 1A), also after adjusting for age, IPI, and WHO performance score (supplemental Table 6). T-cell differentiation states (naïve, stem cell memory, central memory, effector memory T cells, and terminally differentiated effector memory T cells re-expressing CD45RA) did not significantly differ between both lymphoma subtypes (supplemental Figure 4B). $CD4^+CD127^+$ T cells were increased in both lymphoma subtypes compared with HDs (Figure 1B), but only patients with DLBCL NOS had lower frequencies of $CD8^+CD127^+$ cytotoxic T cells than patients with HGBL-*MYC/BCL2* and HDs (Figure 1B).

Increased activated T cells predominantly in patients with HGBL-*MYC/BCL2*

Both lymphoma subtypes displayed increased $CD4^+$ and $CD8^+$ HLA-DR^+ T-cell and $CD4^+CD38^+$ T-cell frequencies compared with HDs, but patients with DLBCL NOS had reduced $CD8^+CD38^+$ T-cell frequencies compared with those with HGBL-*MYC/BCL2* and HDs (Figure 1D). FlowSOM analysis of T-cell populations confirmed increased "activated" $CD8^+$ and $CD4^-CD8^-$ T cells coexpressing PD-1, CD38, and HLA-DR in patients with HGBL-*MYC/BCL2* compared with patients with DLBCL NOS (Figure 1C; supplemental Figure 5A). Additionally, $CD4^+CD25^+$ T cells were increased in patients with HGBL-*MYC/BCL2* (Figure 1C; supplemental Figure 4C).

Increased PD-1^+CD8^+ cells in patients with HGBL-*MYC/BCL2* vs increased T-cell senescence in patients with DLBCL NOS

Next, we evaluated T-cell exhaustion state focusing on the expression of important coinhibitory molecules TIM-3, TIGIT, LAG-3, and PD-1. Frequencies of $CD4^+$ and $CD8^+$ T cells expressing TIM-3 did not significantly differ between patients with HGBL-*MYC/BCL2* and patients with DLBCL NOS but was increased in both lymphoma subtypes compared with HDs (supplemental Figure 4D).

Patients with HGBL-*MYC/BCL2* exhibited higher frequencies of $CD4^+TIGIT^+$ T cells (supplemental Figure 4E) compared with HDs. There was no difference in LAG-3–expressing T cells between patients with HGBL-*MYC/BCL2* and patients with DLBCL NOS, and only LAG-3 expressing Tregs were decreased in both lymphoma subtypes compared with HDs (supplemental Figure 4F).

Interestingly, PD-1 expression was increased on $CD4^+$ T cells and Tregs in both lymphoma subtypes, but PD-1^+CD8^+ T cells were selectively increased in patients with HGBL-*MYC/BCL2* (Figure 1E). UMAP analysis indicated that T-cells may exhibit coexpression of CD38, HLA-DR, and PD-1 (Figure 1F).

We also analyzed markers of T-cell senescence (defined as loss of costimulatory molecules CD27 and CD28 and gain of KLRG1 and CD57) as another T-cell dysfunctional state that may negatively affect the response to immunotherapeutic approaches. In contrast with T-cell exhaustion, patients with DLBCL NOS exhibited a more senescent phenotype than patients with HGBL-*MYC/BCL2* and HDs, as was reflected in lower $CD27^+$ and $CD28^+$ and higher $KLRG1^+$ and $CD57^+$ T-cell frequencies (supplemental Figure 4G) in various T-cell subsets (Figure 1C; supplemental Figure 5A), independent of age, IPI, and WHO performance score (supplemental Table 6). Interestingly, UMAP analysis indicated that T cells may exhibit coexpression of PD-1, KLRG1, and CD57 (supplemental Figure 4H), underlining the potential differences in T-cell phenotype in HGBL-*MYC/BCL2* (T-cell exhaustion) vs DLBCL NOS (T-cell senescence).

PD-1^+ T cells are functionally impaired in patients with HGBL-*MYC/BCL2*, but total $CD4^+$ and $CD8^+$ T cells have a similar functionality as in patients with DLBCL NOS and HDs

To gain further insight into the exhaustion state of PD-1^+ T cells, we evaluated cytokine secretion profile of T cells after stimulation of

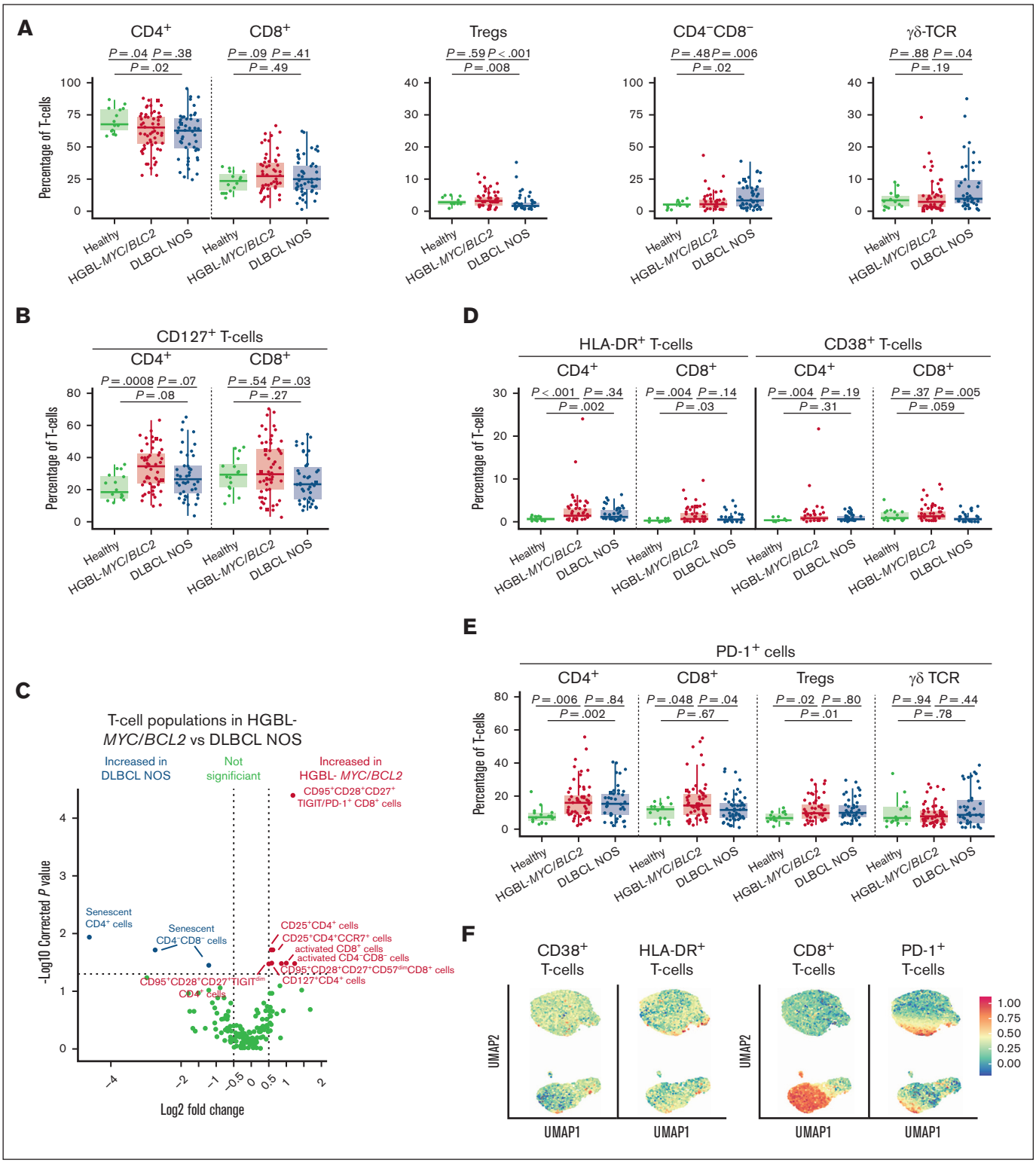

Figure 1. T-cell phenotype in patients with HGBL-*MYC/BCL2*, patients with DLBCL NOS, and HDs. (A-B) Expression analysis of major T-cell subsets (A), and CD127 (B) in HDs (green; n = 16), patients with HGBL-*MYC/BCL2* (red; n = 66), and patients with DLBCL NOS (blue; n = 53). (C) In-depth analysis of the computationally identified T-cell populations by FlowSOM expressed higher (red) or lower (blue) in patients with HGBL-*MYC/BCL2* vs patients with DLBCL NOS. (D-E) Expression analysis of HLA-DR and CD38 (D) and PD-1 (E) in HDs (green; n = 16), patients with HGBL-*MYC/BCL2* (red; n = 66), and patients with DLBCL NOS (blue; n = 53). (F) Dimensionality reduction by UMAP of the flow cytometry data of T-cells. Color overlays for CD38, HLA-DR, PD-1, and CD8 are depicted. For all box plots, the lower upper hinges correspond to the 25th and 75th percentiles. The middle hinge corresponds to the median. The whiskers extend from the largest to smallest value ± 1.58 * interquartile range. Samples are plotted individually, bone marrow samples (n = 3 HGBL-*MYC/BCL2* and n = 1 *DLBCL NOS*) are indicated as square. Nonparametric Mann-Whitney *U* test between 2 groups was used for statistical analysis, in which $P < .05$ was considered significant.

PBMCs with PMA/ionomycin. We detected no overt differences in proliferation (Figure 2A-B), degranulation (Figure 2C), or cytokine secretion (IFN-γ, TNF-α, or IL-2) (supplemental Figure 6A) of total $CD4^+$ and $CD8^+$ T-cell populations from HGBL-*MYC/BCL2*, DLBCL NOS, and HDs. Nonetheless, when we focused solely on PD-1^+ T cells, we observed increased production of IFN-γ by PD-1^+CD8^+ T cells in patients with HGBL-*MYC/BCL2* compared with HDs but not patients with DLBCL NOS (Figure 2D). TNF-α secreted by $CD4^+$PD-1^+ T cells was significantly decreased in patients with HGBL-*MYC/BCL2* compared with patients with DLBCL NOS but not HD, whereas IL-2 secreted by $CD4^+$PD-1^+ T cells was significantly decreased in patients with HGBL-*MYC/BCL2* compared with HD but not patients with DLBCL NOS (Figure 2D). The surface expression of degranulation marker CD107a was also decreased in PD-1^+CD8^+ T cells, but not in PD-1^+CD4^+ (Figure 2E), total $CD4^+$, or total $CD8^+$ T cells (supplemental Figure 6B) in patients with HGBL-*MYC/BCL2* compared with patients with DLBCL NOS and HDs. Thus, cytokine production and degranulation are impaired in PD-1^+ T cells of patients with HGBL-*MYC/BCL2*.

HGBL-*MYC/BCL2* has increased frequencies of NK cells with an activated phenotype, whereas patients with DLBCL NOS have more NK cells expressing inhibiting receptor NKG2A

In the NK-cell compartment, both lymphoma subtypes had a tendency toward a decreased frequency of (cytotoxic) $CD16^+CD56^{dim}$ NK cells and increased frequency of (non-cytotoxic) $CD56^{bright}$ NK cells compared with that in HDs, but these frequencies did not differ between the lymphoma subtypes (Figure 3A).

Patients with DLBCL NOS displayed higher frequencies of NK cells expressing the inhibiting receptor $NKG2A^+$ than patients with HGBL-*MYC/BCL2* and HDs (Figure 3B), even after adjustment for age and WHO performance score. Unsupervised cluster analyses further revealed an increased expression of NK cell population coexpressing NKG2A and NKG2D in patients with DLBCL NOS compared with patients with HGBL-*MYC/BCL2* (Figure 3C; supplemental Figure 5B). UMAP analysis indicated that NK cells may exhibit coexpression of NKG2A, NKG2C, NKG2D, and TIM3 in several possible combinations (supplemental Figure 7A).

Both lymphoma subtypes exhibited lower TIM-3^+– and DNAM-1^+–expressing NK cells than HDs (Figure 3D). Frequencies of HLA-DR^+ $CD56^{dim}$ cells were decreased only in patients with DLBCL NOS compared with those with HGBL-*MYC/BCL2* (Figure 3E). UMAP analysis indicated that the majority of HLA-DR^+ NK cells, but not all, may exhibit coexpression of DNAM-1 (Figure 3E). The frequency of NK cells expressing inhibitory (TIGIT and KLRG1) or maturation (CD57) markers did not significantly differ between both lymphoma subtypes and HDs (supplemental Figure 7B).

In a subset of available samples, NK cells from both lymphoma subtypes and HDs exhibited a similar cytotoxic capacity as determined by their lytic activity against NK cell–susceptible K562 cell line (Figure 3F). However, NK cell degranulation (CD107a surface expression) was significantly lower in the HGBL-*MYC/BCL2* group than in HDs (Figure 3F). Total NK cells and cytotoxic $CD16^+CD56^{dim}$ NK cell frequencies did not significantly differ between the groups and showed no correlation with K562 kill or degranulation (supplemental Figure 7C-D).

Discussion

The efficacy of immunotherapeutic approaches is partly dependent on the quality of host immune cells, which may be affected by lymphoma-intrinsic *MYC*. To investigate this, we characterized peripheral T-cells and NK cells of patients with HGBL-*MYC/BCL2* vs patients with DLBCL NOS early in treatment and age-matched HDs. Our analyses reveal that patients with HGBL-*MYC/BLC2* have a distinct peripheral T-cell and NK cell phenotype from patients with DLBCL NOS, with an increased frequency of functionally impaired PD-1^+CD8^+ T cells. In contrast to patients with DLBCL NOS, patients with HGBL-*MYC/BCL2* did not show increased frequencies of senescent T cells. Although we found no other functional deficiencies in T cells and NK cells of patients with HGBL-*MYC/BCL2* and patients with DLBCL NOS, the increase in PD-1^+CD8^+ T cells indicate a negative impact of lymphoma-intrinsic *MYC* on immune effector T cells.

The increase in activated T cells was associated with T-cell exhaustion, but not senescence, in patients with HGBL-*MYC/BCL2*. On the contrary, in patients with DLBCL NOS, increased T-cell activation was associated with T-cell senescence, even after correction for age. This may suggest that both lymphoma subtypes transition to a different T-cell state after initial (tumor-induced) T-cell activation. Exhausted and senescent cells are generally considered as 2 dysfunctional states of T cells or NK cells, but there are essential differences between these cells in terms of differentiation, metabolism, and, most importantly, effector functions; although both cells have lost their proliferative capacity, senescent cells, in contrast to exhausted cells, have potent cytotoxic activity and secrete proinflammatory cytokines such as IFN-γ and TNF-α after activation.[20,21] Thus, in cancer immunotherapy with monoclonal or bispecific antibodies, senescent cells redirected to tumor cells may still contribute to therapeutic effects, whereas exhausted cells do not. Therefore, the higher proportion of exhausted PD-1^+CD8^+ T cells that are associated with *MYC* rearrangements in our study requires attention by further investigating its impact on response to immunotherapeutic approaches and clinical outcomes.

To optimally guide immunotherapeutic approaches for *MYC*-rearranged HGBL, we compared peripheral blood immune profile of patients with HGBL-*MYC/BCL2* with that of patients with DLBCL NOS without *MYC* rearrangements. It is, however, important to acknowledge the molecular heterogeneity of the disease and its impact on clinical outcomes.[22-26] Our results reveal considerable heterogeneity between patient samples, and differential effects of molecular subtypes on peripheral blood immune cells cannot be ruled out.

In apparent contrast to our results, an earlier study reported decreased $CD56^{bright}$/$CD16^{dim/-}$ NK cells in patients with *MYC*-rearranged lymphoma compared with HDs.[15] Although we found no significant differences in $CD56^{bright}$/$CD16^{dim/-}$ cells between both lymphoma subtypes and HDs, it should be noted that the patients in our cohort had already received 1 cycle of R-CHOP. In fact, our pilot analyses performed in patients with DLBCL NOS revealed that R-CHOP treatment reduces NK cell numbers. When

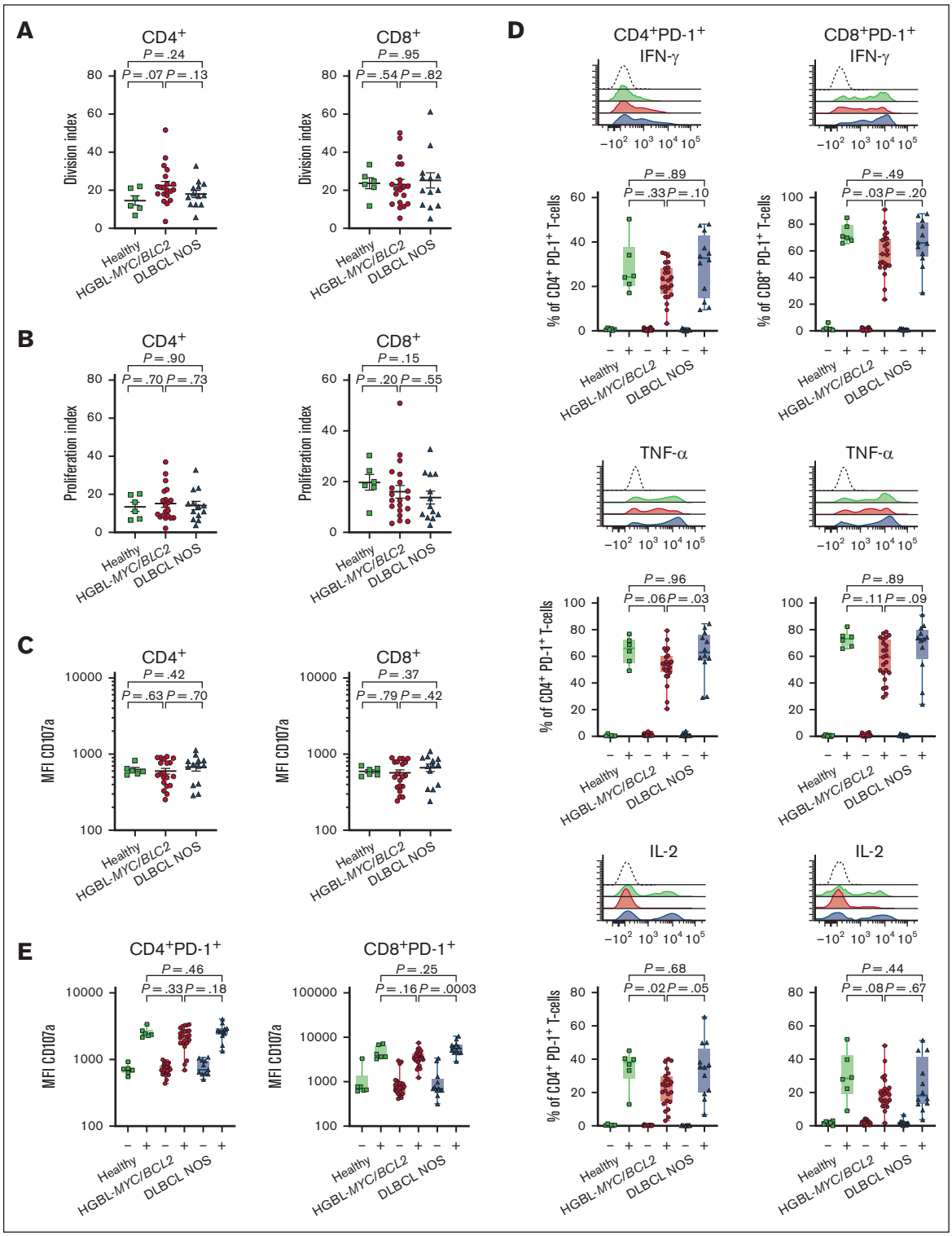

Figure 2. T-cell functionality in patients with HGBL-*MYC/BCL2*, patients with DLBCL NOS, and HDs. (A-B) Percentages of total CD4$^+$ (left panels) and total CD8$^+$ (right panels) T-cell proliferation division index (A) and proliferation index (B) in HDs (green; n = 6), patients with HGBL-*MYC/BCL2* (red; n = 20), and patients with DLBCL NOS (blue; n = 13) after 5 days of stimulation with CD3/CD28 beads. (C) Mean fluorescent intensity (MFI) of CD107a after 5 days of stimulation with CD3/CD28 beads on total CD4$^+$ (left panel) and total CD8$^+$ (right panel) T cells in HDs (green; n = 6), patients with HGBL-*MYC/BCL2* (red; n = 23), and patients with DLBCL NOS (blue; n = 13). (D-E) Representative cytometry histograms and comparative percentages of PD-1$^+$CD4$^+$ (left panels) and PD-1$^+$CD8$^+$ (right panels) T cells for IFN-γ, TNF-α, and IL-2 and (E) MFI of CD107a on PD-1$^+$CD4$^+$ (left panel) and PD-1$^+$CD8$^+$ (right panel) in HDs (green; n = 6), patients with HGBL-*MYC/BCL2* (red; n = 23), and patients with DLBCL NOS (blue; n = 12) after 4-hour stimulation with PMA/ionomysin. − represents unstimulated cells; + represents stimulated cells. Nonparametric Mann-Whitney *U* test was used for statistical analysis, in which $P < .05$ was considered significant.

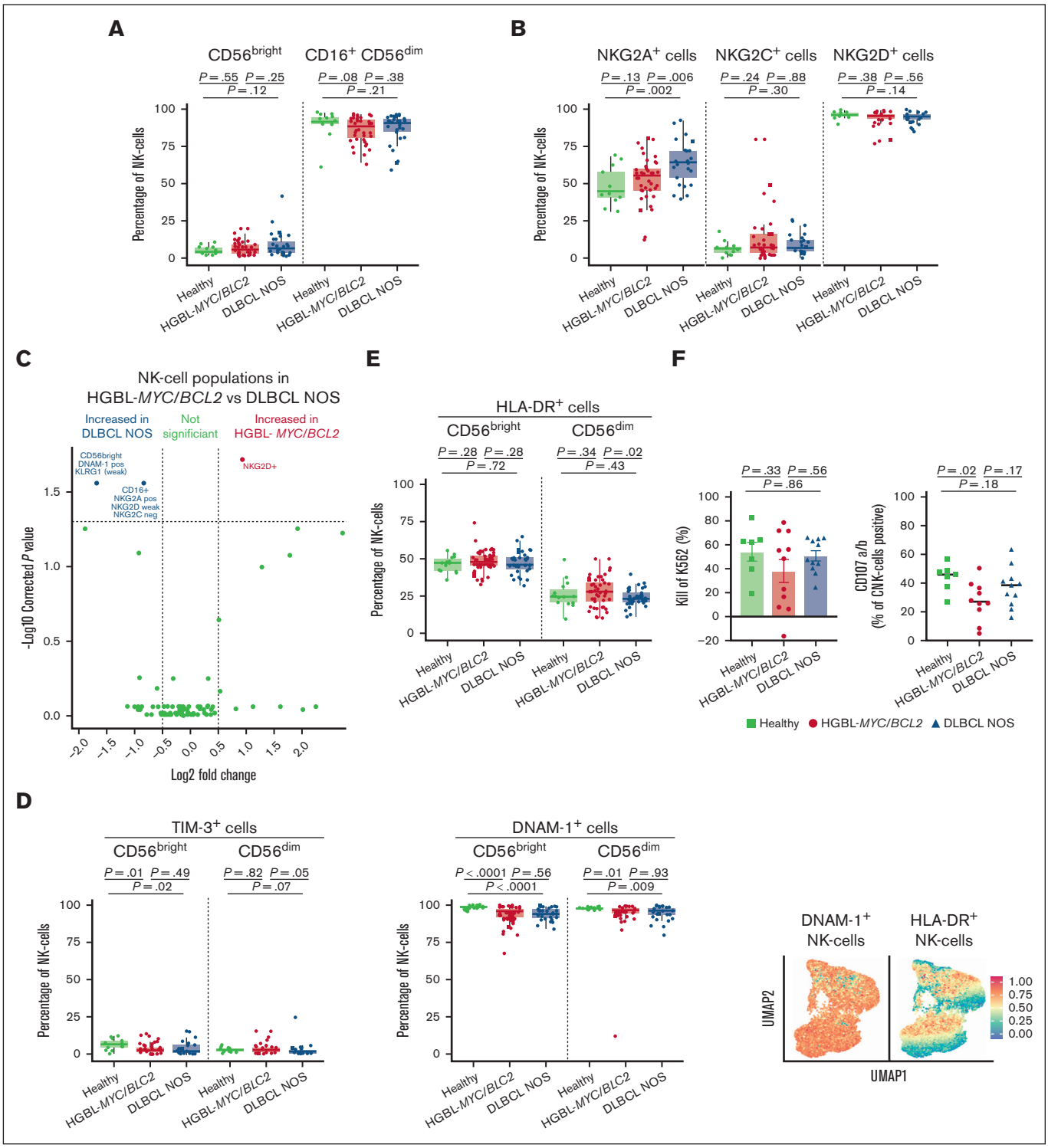

Figure 3. NK cell phenotype in patients with HGBL-*MYC/BCL2*, patients with DLBCL NOS, and HDs. (A-B) Expression analysis of major NK cell subsets (A) and NK cell receptors (B) in HDs (green; n = 15 in A; n = 13 in panel B), patients with HGBL-*MYC/BCL2* (red; n = 51 in A; n = 41 in panel B), and patients with DLBCL NOS (blue; n = 35 in A; n = 25 in panel B). (C) In-depth analysis of the computationally identified NK cell populations by FlowSOM expressed higher (red) or lower (blue) in patients with HGBL-*MYC/BCL2* vs patients with DLBCL NOS. (D-E) Expression analysis of TIM-3, DNAM-1 (D), and HLA-DR (E) on NK cell subsets in HDs (green; n = 13-15), patients with HGBL-*MYC/BCL2* (red; n = 41-51; based on sample availability for the 2 T-cell panels; see also supplemental Figure 1), and patients with DLBCL NOS (blue; n = 25-35) and dimensionality reduction by UMAP of the flow cytometry data of NK cells. Color overlays for DNAM-1 and HLA-DR are depicted. (F) Comparative percentages of kill of K562 and degranulation as measured by CD107a/b surface expression on NK cells in HDs (green; n = 7), patients with HGBL-*MYC/BCL2* (red; n = 11), and patients with DLBCL NOS (blue; n = 11) after 4-hour coculture of PBMCs with K562 cell line. Cytotoxicity is calculated relative to the amount of K562 cells without PBMCs. For all box plots, the lower upper hinges

Figure 3 (continued) correspond to the 25th and 75th percentiles. The middle hinge corresponds to the median. The whiskers extend from the largest to smallest value ± 1.58 * interquartile range. Samples are plotted individually, bone marrow samples (n = 3 HGBL-*MYC/BCL2* and n = 1 DLBCL NOS) are indicated as square. Mann-Whitney *U* test between 2 groups was used for statistical analysis. $P < .05$ was considered significant.

comparing $CD56^{bright}/CD16^{dim/-}$ NK cells in available samples from HDs (n = 15) and patients with DLBCL NOS before R-CHOP (n = 9), we found lower $CD56^{bright}/CD16^{dim/-}$ NK cells in patients with DLBCL NOS, consistent with the earlier report. Thus, full R-CHOP course may affect peripheral immune cell populations, with consequences to the efficacy of second-line immunotherapeutic approaches.[27] Additionally, we cannot rule out the possibility that in the course of R-CHOP, the differences in T-cell subsets between patients with HGBL-*MYC/BCL2* vs patients with DLBCL NOS become more visible, because previous studies showed decreased absolute $CD4^+$ T-cell counts after 6 to 8 cycles of R-CHOP[28] and decreased T-cell metabolism and proliferation after cyclophosphamide exposure.[29]

Although our results indicate a negative impact of lymphoma-intrinsic *MYC* on the peripheral effector immune cells, we believe that the inferior survival outcomes of patients with HGBL-*MYC/BCL2* to R-CHOP cannot be solely attributed to the particular differences in peripheral blood immune profiles found in this study. This idea is strengthened by our findings of no overall functional deficiencies in T cells and NK cells of patients with HGBL-*MYC/BCL2* and patients with DLBCL NOS. Further investigation is warranted to explore other mechanisms contributing to evasion from immune effector cells. For example, an important drawback in the application of immunotherapeutic approaches is the difficulty of immune effector cells to cope with the immunosuppressive cells and factors in the tumor microenvironment. Within this regard, *MYC* is highly relevant because lymphoma-intrinsic *MYC* plays specific and crucial roles in reshaping the immunosuppressive microenvironment. For example, *MYC* contributes to evading both innate and adaptive antitumor immune responses in the tumor microenvironment, as we and others have reviewed before.[30-32] This is suggested by experimental and clinical evidence that the overexpression of lymphoma-intrinsic *MYC* and subsequent target genes clinically associates with less favorable responses toward the CD20 × CD3 bispecific antibody glofitamab in patients with BCL.[33] Possibly, the exhausted T cells observed in our study may be more pronounced in the tumor microenvironment of patients with *MYC* rearrangement. Future studies should further elucidate the infiltration, differentiation status, and function of immune effector T cells and NK cells in the microenvironment of patients with HGBL-*MYC/BCL2*.

Finally, it is important to emphasize that our results are applicable to peripheral blood immune profiles of patients with HGBL-*MYC/BCL2* and patients with DLBCL in first-line therapy. Therefore, our results may be particularly relevant for upcoming immunotherapeutic approaches as potential first-line (combination) treatment strategies, such as T-cell–engaging bispecifcs.[34] For second- or third-line immunotherapeutic approaches, such as chimeric antigen receptor T-cell therapy, further characterization of T cells and NK cells during or after first-line immunochemotherapy regimens (R-CHOP or DA-EPOCH-R) are needed.

In conclusion, we demonstrated that patients with HGBL-*MYC/BCL2* and patients with DLBCL NOS without a *MYC* rearrangement have distinct peripheral blood T-cell and NK-cell profiles. Our results provide valuable insights into the potential of T-cell– and NK-cell–based immunotherapeutic approaches in aggressive BCLs.

Authorship

Contribution: A.V.d.J., M.E.D.C., and T.M. designed the research; C.D. performed computation FlowSOM analysis; W.S.C.B. designed the flow cytometry panels; A.V.d.J., C.D., W.S.C.B., C.L.B.M.K., R.R., M.C., M.E., and I.T. performed the experiments; A.V.d.J. analyzed the data under the supervision of M.G.M.R., M.E.D.C., and T.M.; E.v.W. provided statistical support; M.N., M.W.M.v.d.P., K.d.H., C.P.W.K., L.S., M.O., R.B., and H.R.K. contributed to the data collection; A.V.d.J. and T.M. wrote the first draft of the manuscript with a critical writing-review from M.G.M.R. and M.E.D.C. and contributions from all authors; and all authors approved the final version of the manuscript.

Conflict-of-interest disclosure: M.N. received research support from Takeda and has an advisory role at AbbVie. M.E.D.C. received research support from AbbVie, Genmab, Bristol Myers Squibb, and Gilead, and has an advisory role at AbbVie, Novartis, and Incyte. T.M. received research funding from Takeda, Janssen, and Genmab. The remaining authors declare no competing financial interests.

ORCID profiles: A.V.d.J., 0000-0002-5397-1762; W.S.C.B., 0000-0002-4074-9257; R.R., 0009-0008-3317-437X; M.N., 0000-0002-2740-2873; M.O., 0000-0002-6742-9261; E.v.W., 0000-0001-7469-7427; T.M., 0000-0002-5557-7187.

Correspondence: Tuna Mutis, VU University Medical Center Amsterdam, Hematology, de Boelelaan 1117, P.O. Box 7057, Amsterdam 1007 MB, The Netherlands; email: t.mutis@amsterdamumc.nl.

References

1. Alaggio R, Amador C, Anagnostopoulos I, et al. The 5th edition of the World Health Organization classification of haematolymphoid tumours: lymphoid neoplasms. *Leukemia*. 2022;36(7):1720-1748.
2. Savage KJ, Johnson NA, Ben-Neriah S, et al. MYC gene rearrangements are associated with a poor prognosis in diffuse large B-cell lymphoma patients treated with R-CHOP chemotherapy. *Blood*. 2009;114(17):3533-3537.
3. Barrans S, Crouch S, Smith A, et al. Rearrangement of MYC is associated with poor prognosis in patients with diffuse large B-cell lymphoma treated in the era of rituximab. *J Clin Oncol*. 2010;28(20):3360-3365.

4. McPhail ED, Maurer MJ, Macon WR, et al. Inferior survival in high-grade B-cell lymphoma with MYC and BCL2 and/or BCL6 rearrangements is not associated with MYC/IG gene rearrangements. *Haematologica*. 2018;103(11):1899-1907.
5. Hutchings M, Mous R, Clausen MR, et al. Dose escalation of subcutaneous epcoritamab in patients with relapsed or refractory B-cell non-Hodgkin lymphoma: an open-label, phase 1/2 study. *Lancet*. 2021;398(10306):1157-1169.
6. Bannerji R, Arnason JE, Advani RH, et al. Odronextamab, a human CD20xCD3 bispecific antibody in patients with CD20-positive B-cell malignancies (ELM-1): results from the relapsed or refractory non-Hodgkin lymphoma cohort in a single-arm, multicentre, phase 1 trial. *Lancet Haematol*. 2022;9(5):e327-e339.
7. Dickinson MJ, Carlo-Stella C, Morschhauser F, et al. Glofitamab for relapsed or refractory diffuse large B-cell lymphoma. *N Engl J Med*. 2022;387(24):2220-2231.
8. Neelapu SS, Locke FL, Bartlett NL, et al. Axicabtagene ciloleucel CAR T-cell therapy in refractory large B-cell lymphoma. *N Engl J Med*. 2017;377(26):2531-2544.
9. Locke FL, Ghobadi A, Jacobson CA, et al. Long-term safety and activity of axicabtagene ciloleucel in refractory large B-cell lymphoma (ZUMA-1): a single-arm, multicentre, phase 1-2 trial. *Lancet Oncol*. 2019;20(1):31-42.
10. Schuster SJ, Bishop MR, Tam CS, et al. Tisagenlecleucel in adult relapsed or refractory diffuse large B-cell lymphoma. *N Engl J Med*. 2019;380(1):45-56.
11. Abramson JS, Palomba ML, Gordon LI, et al. Lisocabtagene maraleucel for patients with relapsed or refractory large B-cell lymphomas (TRANSCEND NHL 001): a multicentre seamless design study. *Lancet*. 2020;396(10254):839-852.
12. Bai R, Chen N, Li L, et al. Mechanisms of cancer resistance to immunotherapy. *Front Oncol*. 2020;10:1290.
13. Binnewies M, Roberts EW, Kersten K, et al. Understanding the tumor immune microenvironment (TIME) for effective therapy. *Nat Med*. 2018;24(5):541-550.
14. Swaminathan S, Hansen AS, Heftdal LD, et al. MYC functions as a switch for natural killer cell-mediated immune surveillance of lymphoid malignancies. *Nat Commun*. 2020;11(1):2860.
15. Amini RM, Enblad G, Hollander P, et al. Altered profile of immune regulatory cells in the peripheral blood of lymphoma patients. *BMC Cancer*. 2019;19(1):316.
16. Lei T, Wu G, Xu Y, et al. Peripheral immune cell profiling of double-hit lymphoma by mass cytometry. *BMC Cancer*. 2023;23(1):184.
17. Swerdlow SH, Campo E, Pileri SA, et al. The 2016 revision of the World Health Organization classification of lymphoid neoplasms. *Blood*. 2016;127(20):2375-2390.
18. Emmaneel A, Quintelier K, Sichien D, et al. PeacoQC: peak-based selection of high quality cytometry data. *Cytometry A*. 2022;101(4):325-338.
19. Roederer M. Interpretation of cellular proliferation data: avoid the panglossian. *Cytometry A*. 2011;79(2):95-101.
20. Akbar AN, Henson SM, Lanna A. Senescence of T lymphocytes: implications for enhancing human immunity. *Trends Immunol*. 2016;37(12):866-876.
21. Pereira BI, De Maeyer RPH, Covre LP, et al. Sestrins induce natural killer function in senescent-like CD8(+) T cells. *Nat Immunol*. 2020;21(6):684-694.
22. Alizadeh AA, Eisen MB, Davis RE, et al. Distinct types of diffuse large B-cell lymphoma identified by gene expression profiling. *Nature*. 2000;403(6769):503-511.
23. Reddy A, Zhang J, Davis NS, et al. Genetic and functional drivers of diffuse large B cell lymphoma. *Cell*. 2017;171(2):481-494.e15.
24. Schmitz R, Wright GW, Huang DW, et al. Genetics and pathogenesis of diffuse large B-cell lymphoma. *N Engl J Med*. 2018;378(15):1396-1407.
25. Chapuy B, Stewart C, Dunford AJ, et al. Molecular subtypes of diffuse large B cell lymphoma are associated with distinct pathogenic mechanisms and outcomes. *Nat Med*. 2018;24(5):679-690.
26. Wright GW, Huang DW, Phelan JD, et al. A probabilistic classification tool for genetic subtypes of diffuse large B cell lymphoma with therapeutic implications. *Cancer Cell*. 2020;37(4):551-568.e14.
27. Dubnikov Sharon T, Assayag M, Avni B, et al. Early lymphocyte collection for anti-CD19 CART production improves T-cell fitness in patients with relapsed/refractory diffuse large B-cell lymphoma. *Br J Haematol*. 2023;202(1):74-85.
28. Ito K, Okamoto M, Inaguma Y, et al. Influence of R-CHOP therapy on immune system restoration in patients with B-cell lymphoma. *Oncology*. 2016;91(6):302-310.
29. Das RK, O'Connor RS, Grupp SA, Barrett DM. Lingering effects of chemotherapy on mature T cells impair proliferation. *Blood Adv*. 2020;4(19):4653-4664.
30. Whitfield JR, Soucek L. Tumor microenvironment: becoming sick of Myc. *Cell Mol Life Sci*. 2012;69(6):931-934.
31. de Jonge AV, Mutis T, Roemer MGM, Scheijen B, Chamuleau MED. Impact of MYC on anti-tumor immune responses in aggressive B cell non-Hodgkin lymphomas: consequences for cancer immunotherapy. *Cancers (Basel)*. 2020;12(10):3052.
32. Li J, Dong T, Wu Z, Zhu D, Gu H. The effects of MYC on tumor immunity and immunotherapy. *Cell Death Discov*. 2023;9(1):103.
33. Bröske AME, Korfi K, Belousov A, et al. Pharmacodynamics and molecular correlates of response to glofitamab in relapsed/refractory non-Hodgkin lymphoma. *Blood Adv*. 2022;6(3):1025-1037.
34. Falchi L, Vardhana SA, Salles GA. Bispecific antibodies for the treatment of B-cell lymphoma: promises, unknowns, and opportunities. *Blood*. 2023;141(5):467-480.